VSP

Advanced Composite Materials 18 (2009) 265–285

ADVANCED COMPOSITE MATERIALS
www.brill.nl/acm

Tension–Compression Asymmetry in the Off-Axis Nonlinear Rate-Dependent Behavior of a Unidirectional Carbon/Epoxy Laminate at High Temperature and Incorporation into Viscoplasticity Modeling

M. Kawai [a,*], **J. Q. Zhang** [b], **S. Saito** [b], **Y. Xiao** [c] **and H. Hatta** [d]

[a] Department of Engineering Mechanics and Energy, University of Tsukuba, Tsukuba 305-8573, Japan

[b] Graduate School of Systems and Information Engineering, University of Tsukuba, Tsukuba 305-8573, Japan

[c] Aerospace Research and Development Directorate, Japan Aerospace Exploration Agency, Mitaka 181-0015, Japan

[d] Institute of Space and Astronautical Science, Japan Aerospace Exploration Agency, Sagamihara 229-8510, Japan

Received 17 July 2008; accepted 20 August 2008

Abstract

Off-axis compressive deformation behavior of a unidirectional CFRP laminate at high temperature and its strain-rate dependence in a quasi-static range are examined for various fiber orientations. By comparing the off-axis compressive and tensile behaviors at an equal strain rate, the effect of different loading modes on the flow stress level, rate-dependence and nonlinearity of the off-axis inelastic deformation is elucidated. The experimental results indicate that the compressive flow stress levels for relatively larger off-axis angles of 30°, 45° and 90° are about 50 percent larger than in tension for the same fiber orientations, respectively. The nonlinear deformations under off-axis tensile and compressive loading conditions exhibit significant strain-rate dependence. Similar features are observed in the fiber-orientation dependence of the off-axis flow stress levels under tension and compression and in the off-axis flow stress differential in tension and compression, regardless of the strain rate. A phenomenological theory of viscoplasticity is then developed which can describe the tension–compression asymmetry as well as the rate dependence, nonlinearity and fiber orientation dependence of the off-axis tensile and compressive behaviors of unidirectional composites in a unified manner. It is demonstrated by comparing with experimental results that the proposed viscoplastic constitutive model can be applied with reasonable accuracy to predict the different, nonlinear and rate-dependent behaviors of the unidirectional composite under off-axis tensile and compressive loading conditions.

* To whom correspondence should be addressed. E-mail: mkawai@kz.tsukuba.ac.jp
Edited by JSCM

DOI:10.1163/156855109X434702

Keywords
Unidirectional composites, off-axis tension, off-axis compression, nonlinear behavior, rate dependence, tension–compression asymmetry, viscoplastic constitutive model, high temperature, carbon fiber, epoxy

1. Introduction

Reliable application of carbon fiber-reinforced polymer matrix composite (CFRP) laminates to a wide range of structural members that can sustain not only predominant tensile load but also mostly compressive load or combined compressive and tensile load in bending is required for improvement in the overall performance and durability of CFRP structures. To take full advantage of the superior properties of CFRPs in the design of compression, compression–tension and tension members, we need to properly understand the similarities and differences between their mechanical behaviors under tensile and compressive loading conditions. In addressing the issue of distinguishing between the behaviors of CFRP laminates loaded in different directions, we should also consider their matrix-dominated behavior which is the key to accurate evaluation of their performance and durability [1], since composite laminates are locally subjected to off-axis loading either in tension or compression during their service and some damage easily develops in such locations.

Matrix polymers in their glassy states show nonlinear responses to a shear load, and the resulting shear deformations depend on the time and rate of loading, especially at a high temperature below the glass transition temperatures [2–6]. It is also known that solid polymers often exhibit different behaviors in tension and compression [7]. These facts on the deformation characteristics of polymers suggest that the matrix-dominated deformation behavior of unidirectional CFRP laminates under off-axis loading conditions is also significantly influenced not only by the rate of loading and the orientation of fibers, but also by the mode of loading over a wide range of temperature. For an efficient design by analysis of CFRP components, therefore, it is a prerequisite to establish an engineering constitutive model which allows accurate prediction of the matrix-dominated nonlinear rate-dependent behaviors of CFRP laminates under off-axis tensile and compressive loading conditions.

The effect of loading rate on the off-axis nonlinear stress–strain behavior of unidirectional CFRP laminates has been examined in several studies [8–11]. Gates and Sun [8] investigated the strain-rate dependence of the high-temperature tensile behavior of unidirectional AS4/PEEK laminates using off-axis coupon specimens. Kawai *et al.* [9] observed the high-temperature off-axis tensile behavior of similar unidirectional AS4/PEEK laminates under stress-controlled conditions, and compared it with that under strain-controlled conditions. In the studies by Sun and Yoon [10], the effect of the change in strain rate on the off-axis tensile behavior of unidirectional AS4/PEEK laminates was elucidated, together with the influence of test temperature. Tsai and Sun [11] examined the strain rate dependence of the off-axis

compressive behavior of unidirectional composites in a range of high strain rate by means of SHPB testing.

Macromechanical modeling of the nonlinear rate-dependent behavior of unidirectional composites, which is required for efficient ply-by-ply basis analysis of composite laminates and structures, has extensively been attempted by Sun and coworkers. Gates and Sun [8] extended the one-parameter plasticity model [12] to develop a plane-stress viscoplasticity model based on the overstress concept. Yoon and Sun [13] extended the Bodner–Partom model [14] so as to describe the viscoplastic behavior of unidirectional composites with the help of the effective stress and inelastic strain defined by Sun and Chen [12]. Wang and Sun [15] elaborated the evolution equation of the scalar internal variable assumed in the Gates–Sun model. The comparison with experimental results has demonstrated that the Gates–Sun model [8], Yoon–Sun model [13] and Wang–Sun model [15] can adequately describe the nonlinear rate-dependent deformation of unidirectional PMC laminates under off-axis monotonic loading conditions in a quasi-static strain-rate range. Recently, it has also been elucidated that these rate-dependent plasticity models can successfully be applied to description of the high strain-rate off-axis deformation of unidirectional composites for the range of strain rate attainable in the SHPB experiments [11].

To the best of the present authors' knowledge, however, very few studies are available in which the similarities and differences between the nonlinear rate-dependent deformation behaviors of unidirectional CFRP laminates under off-axis tensile and compressive loading conditions have been examined for different fiber orientations. Thus, the extent of the off-axis flow stress differential at different strain rates in tension and compression has not fully been quantified for unidirectional CFRP laminates. Due to a dearth of available data, a unified constitutive model that allows prediction of the different flow stress levels under off-axis tension and compression besides description of the rate-dependence, nonlinearity and fiber-orientation dependence of the off-axis deformation behavior has not been established. These facts suggest that further basic investigation is required on the inelastic flow behaviors of unidirectional CFRP laminates under off-axis tensile and compressive loading conditions, with a view to developing an efficient engineering constitutive model that takes into account the loading mode dependence as well as the rate-dependence in their matrix-dominated nonlinear inelastic deformation behavior.

In the present study, the off-axis compressive deformation behavior of a unidirectional CFRP laminate at high temperature and its strain-rate dependence in a quasi-static range are examined for various fiber orientations. Off-axis compression tests are performed at two different strain rates for each fiber orientation to observe the strain rate dependence as well as fiber-orientation dependence of the off-axis compressive deformation. To quantify the difference in flow stress level between the off-axis tensile and compressive inelastic deformations, the off-axis compression test results are compared with the off-axis tension test results obtained at the same

strain rates. Then, a phenomenological viscoplasticity model that can describe the tension–compression asymmetry in the off-axis nonlinear rate-dependent behavior of unidirectional composites is developed. Validity of the proposed viscoplasticity model is evaluated by comparing with experimental results.

2. Material and Experimental Procedure

2.1. Material and Specimens

The material used in this study was a unidirectional carbon/epoxy laminate fabricated from the prepreg tape T800H/2500 (P2053F-17, TORAY). The lay-up of virgin laminates was $[0]_{12}$, and they were cured at 130°C in an autoclave. The thickness of as-cured laminates was 2 mm.

Six kinds of coupon specimens with different fiber orientations ($\theta = 0°$, 10°, 15°, 30°, 45°, 90°) were cut from 400 mm by 400 mm unidirectional laminate panels. For static tension tests, the specimen geometry and dimensions based on the testing standard JIS K7073 [16] were adopted; as shown in Fig. 1(a), the dimensions were length $L = 200$ mm, gauge length $L_G = 100$ mm and width $W = 20$ mm ($W = 10$ mm for $\theta = 0°$). For static compression tests, shorter specimens shown in Fig. 1(b) were used to reduce the risk of buckling; the dimensions were length $L = 100$ mm, gauge length $L_G = 10$ mm and width $W = 10$ mm. The nominal dimensions of the short specimens were determined on the basis of the testing standard JIS K7076 [17] and the report of Haberle and Matthews [18] for suitable compression testing on composite laminates. Rectangular-shaped tabs made of aluminum alloy were glued on both ends of specimens with epoxy adhesive (Araldite) in order to protect the gripped portions of the specimens; the thickness of tabs was 1.0 mm for long specimens and 2.0 mm for short specimens. To obtain sufficient adhesion, the adhesive was cured at 90°C for 1 h in a heating chamber (Gravity Oven LG-112, ESPEC).

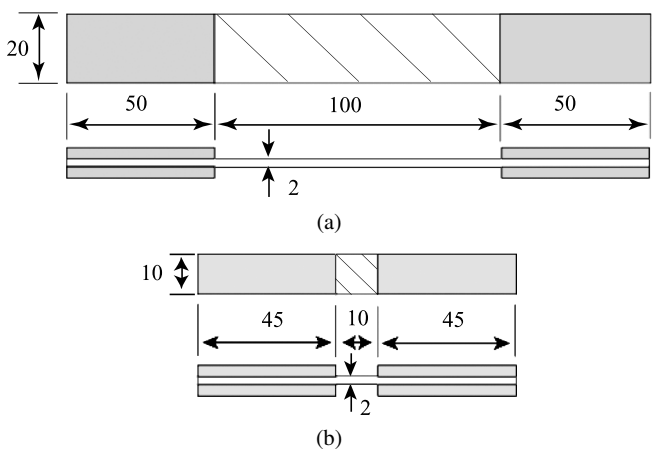

Figure 1. Specimen geometry (dimensions in mm): (a) gauge length 100 mm; (b) gauge length 10 mm.

2.2. Testing Procedure

Off-axis monotonic tension and compression tests were performed at 100°C under stroke control. Two different constant values of nominal strain rate, 10 and 0.1%/min, were chosen for both the off-axis tension and compression tests; these nominal strain rates correspond to the constant crosshead rates of 10 and 0.1 mm/min for long specimens ($L_G = 100$ mm), and 1.0 and 0.01 mm/min for short specimens ($L_G = 10$ mm), respectively. These static tests were conducted on a closed-loop hydraulic MTS-810 testing machine. To raise the temperature of specimens, a heating chamber with a precise digital control capability was employed. The specimens were clamped in the heating chamber by the high temperature hydraulic wedge grips fitted on the testing machine. The specimens were heated up to the test temperature of 100°C in air keeping load at zero, and they were preconditioned in the test environment for 60 min prior to being tested. The variation of the specimen temperature in time from the prescribed value was less than 1.0°C. No attempt was made to control humidity in the chamber. The compression tests on the short specimens were performed with no anti-bucking guides. The longitudinal strain of specimens was measured by strain gauges with a gauge length of 2 mm for tension and 1 mm for compression, and the strain gauges were mounted back to back at the center of each specimen.

3. Experimental Results and Discussion

The in-plane specimen coordinate system is denoted as (x, y), and the x-axis is taken in the loading direction. The principal axes of material anisotropy, i.e., the fiber coordinate system, for unidirectional plies are expressed as $(1, 2)$; the 1-axis being in the fiber direction.

3.1. Off-Axis Stress–Strain Relationships

Axial stress–strain relationships (σ_x–ε_x) obtained from the tension tests at a constant strain rate of 10%/min are shown in Fig. 2 for all fiber orientations $\theta = 0°, 10°, 15°, 30°, 45°$ and 90°. The longitudinal tensile stress–strain relationship ($\theta = 0°$) was almost linear and smooth to final failure, while for the off-axis fiber orientations $\theta = 10°, 15°, 45°$ and 90°, remarkable nonlinearity was observed in the range following the initial linear response. The off-axis stress–strain relationships were in order of fiber orientation angle, and the flow stress required to continue the off-axis deformation became lower with increasing fiber orientation angle. These features of the off-axis tensile behavior are similar to those reported so far in references [8–12, 15].

In the compressive stress–strain relationships shown in Fig. 3, similar nonlinearity and fiber-orientation dependence can be seen. A feature that distinguishes the off-axis compressive behavior in Fig. 3 from the off-axis tensile behavior in Fig. 2 is that the stress–strain relationship for $\theta = 90°$ crossed with that for $\theta = 45°$ in

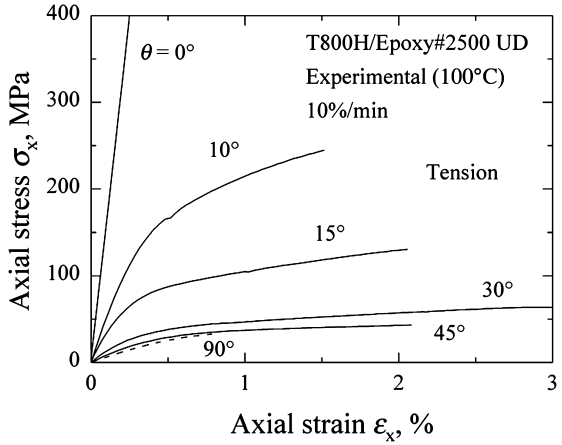

Figure 2. Off-axis tensile stress–strain curves (10%/min).

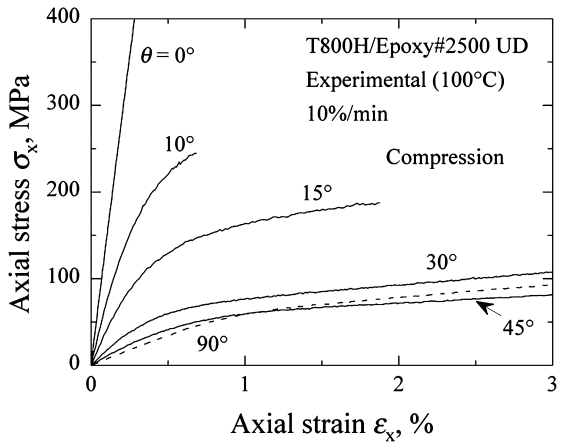

Figure 3. Off-axis compressive stress–strain curves (10%/min).

the compression tests. This phenomenon may be interpreted as follows. When tensile load is given to the transverse direction ($\theta = 90°$) of a coupon specimen of a unidirectional CFRP laminate, it is commonly fractured at a low strain just after transition from initial elastic response to the subsequent nonlinear one. In the case of transverse compression, by contrast, the ultimate failure is retarded due to the suppression of separation failure by the transverse compressive stress, which allows the axial stress in the 90° specimen to ultimately reach a higher level than in the 45° specimen. The effect of the suppression of separation failure due to the action of transverse compressive stress is also reflected by the increase in failure strains, especially for the fiber orientations $\theta = 30$ and 45°.

3.2. Comparison Between Off-Axis Tensile and Compressive Stress–Strain Curves

Figure 4(a)–4(e) shows comparisons between the off-axis tensile and compressive stress–strain curves obtained at the constant rate of 10%/min for all fiber orienta-

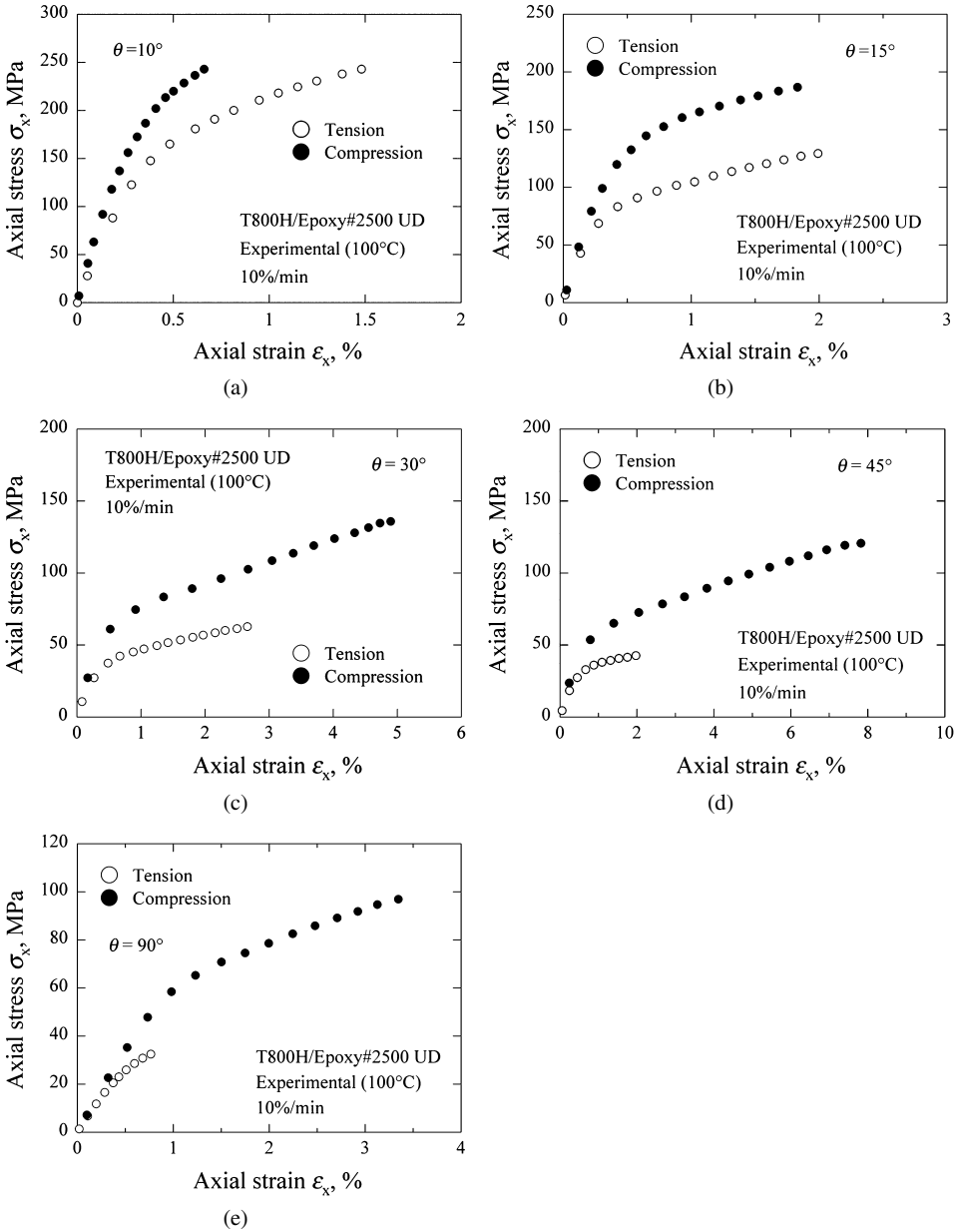

Figure 4. Comparison of off-axis stress–strain curves in tension and compression (10%/min): (a) $\theta = 10°$; (b) $\theta = 15°$; (c) $\theta = 30°$; (d) $\theta = 45°$; (e) $\theta = 90°$.

tions, respectively. The off-axis flow stress level is higher in compression than in tension, regardless of the fiber orientation. More specifically, the off-axis compressive flow stress level became larger by 32% ($\theta = 10°$), 46% (15°), 63% (30°), 69% (45°) and 48% (90°), respectively. It was also observed that the ratio of compressive

Table 1.
Apparent Young's modulus in tension and compression (10%/min)

Angle (°)	E_χ (GPa)	
	Tension	Compression
0	163.5	146.6
10	65.4	72.0
15	38.1	39.2
30	14.7	17.7
45	8.8	10.3
90	6.5	6.9

flow stress to tensile one tends to become larger with increasing fiber orientation angle.

The difference between the apparent elastic moduli in tension and compression for a given fiber orientation is not clear on the figure at a glance. However, it becomes clear by comparison of the values of tensile and compressive Young's moduli that are listed in Table 1. The Young's modulus for $\theta = 0°$ was about 10% lower in compression than in tension, while it was larger in compression for the other fiber orientations by about 10% (10°), 3% (15°), 20% (30°), 17% (45°) and 6% (90°), respectively.

A lower Young's modulus in compression than in tension for loading in the fiber direction was observed elsewhere, and it is likely to be influenced by fiber waviness [19]. By contrast, a larger stiffness in off-axis and transverse compression may be ascribed to the tendency of polymer matrix to exhibit a larger stiffness in compression and the action of transverse compressive stress along fibers besides a higher end constraint on the deformation of the short specimens used for the compression tests.

Note that the stress–strain curves plotted in Fig. 3 are those for the specimens fractured in distinctive compressive failure mode. The same off-axis compression tests were performed on four specimens for each fiber orientation. Only a single kind of failure mode which consisted of in-plane and out-of-plane shear failure (i.e., transverse compressive failure) was observed for the fiber orientations $\theta = 30°, 45°$ and 90°. For each of these fiber orientations, the stress–strain relationships obtained from different specimens agreed well with each other. In contrast, two kinds of different failure modes, an in-plane shear mode and an in-plane kink mode, were observed for each of the specimens with small off-axis angles ($\theta = 10°$ and 15°). The compressive flow stress levels for the specimens fractured in those two kinds of failure modes were significantly different; the off-axis compressive flow stress level for the specimens failed in the in-plane shear mode was lower than those for the specimens failed in the in-plane kink mode. It was also confirmed that the off-axis compressive stress–strain curves for the specimens failed in the in-plane shear mode

agreed well with those obtained from tension tests for the same fiber orientation, which is presumably due to a similar mechanism of deformation. More detailed discussion about the off-axis fracture strength and governing failure mechanisms in tension and compression will be presented in a companion paper [20].

3.3. Strain-Rate Dependence of Off-Axis Tensile and Compressive Behavior

Comparisons of the off-axis tensile stress–strain curves obtained at two different constant strain rates of 10%/min and 0.1%/min are shown in Fig. 5(a)–5(e) for all fiber orientations $\theta = 10, 15, 30, 45$ and 90°, respectively. The flow stress at the strain rate of 0.1%/min was smaller than that at the higher strain rate of 10%/min for all fiber orientations except for the fiber direction, clearly indicating the strain-rate dependence of the off-axis matrix-dominated tensile deformation. More specifically, the axial flow stress level at the lower strain rate of 0.1%/min was reduced by about 38% (10°), 32% (15°), 43% (30°), 54% (45°) and 49% (90°), respectively. It was noticeable that the strain range for initial linear response at the lower strain rate of 0.1%/min was very narrow and the nonlinear deformation was induced by a low stress, regardless of the off-axis fiber orientation.

The rate dependence of the off-axis nonlinear deformation behavior under compression, which can be seen in Fig. 6(a)–6(e), was similar to that under tension. The reduction in axial compressive flow stress at 0.1%/min relative to the value at 10%/min was about 42% (10°), 41% (15°), 34% (30°), 33% (45°) and 42% (90°), respectively. This observation revealed that the strain rate dependence of the off-axis compressive behavior was comparable to that of the off-axis tensile behavior.

It was seen that the fiber-orientation dependence of the off-axis tensile and compressive deformation and the off-axis flow stress differential at the lower rate of 0.1%/min in tension and compression were similar to those at the higher rate of 10%/min. The apparent Young's moduli obtained from the tension and compression tests at 0.1%/min are listed in Table 2. For reference, the lateral contraction and expansion due to the Poisson' effect are shown in Fig. 7(a) and 7(b) for the fiber orientations $\theta = 15°$ and 90°, respectively.

4. A Viscoplasticity Model Considering Tension–Compression Asymmetry

The test results mentioned above allow the quantification of the rate-dependence, nonlinearity and tension–compression asymmetry of the inelastic deformation behavior of the unidirectional carbon/epoxy laminate under off-axis loading conditions. This observation motivates one to develop an inelastic constitutive model that can describe all of these characteristic features in a form applicable to structural analysis of composite laminates. The macroscopic viscoplastic constitutive models developed so far were successfully applied to description of the rate-dependent inelastic behaviors of different kinds of unidirectional composites [8–12, 21–24]. However, they cannot distinguish between the tensile and compressive viscoplastic deformation behaviors for a given off-axis fiber orientation. This is because they

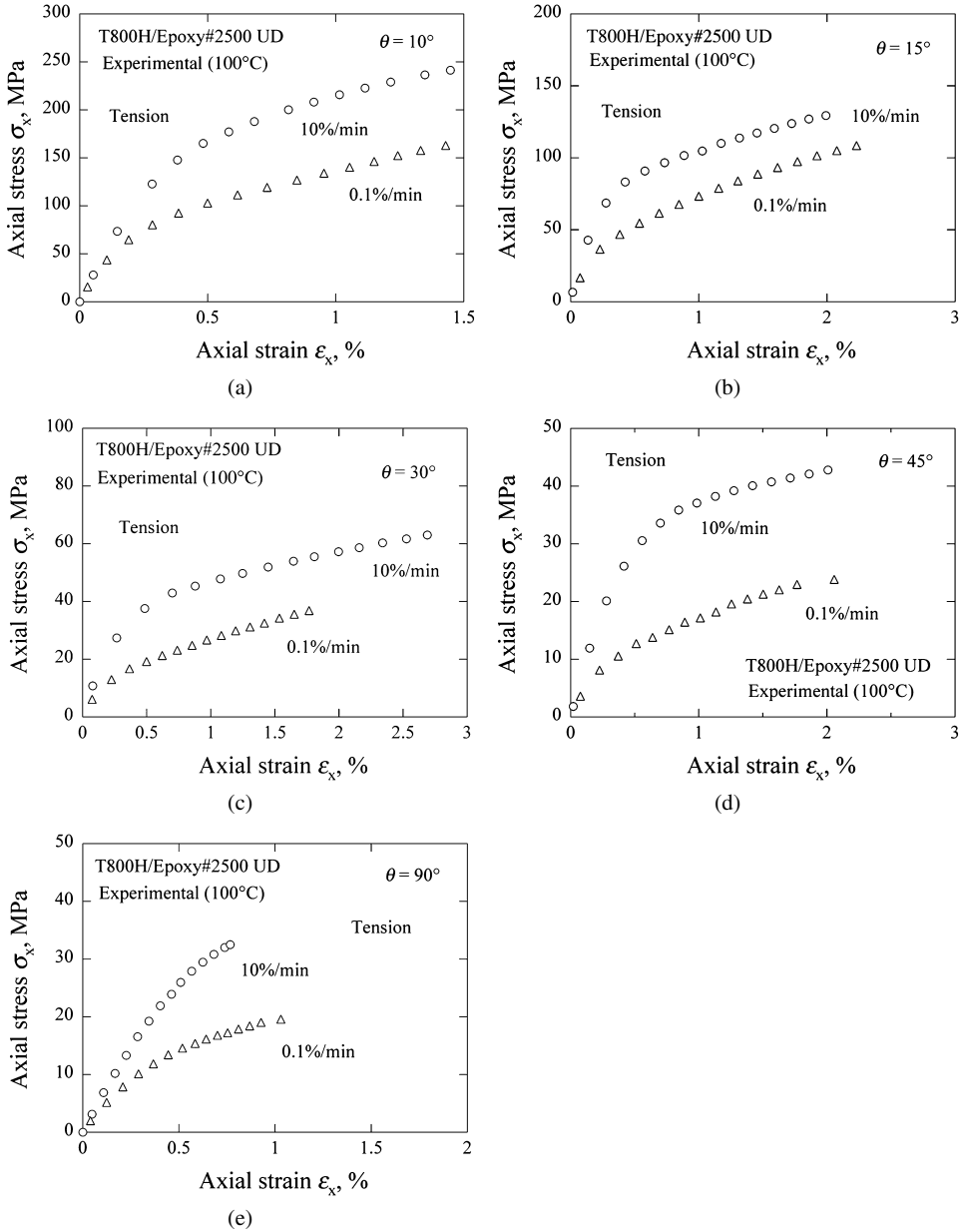

Figure 5. Comparison of off-axis tensile stress–strain curves at different strain rates (10%/min, 0.1%/min): (a) $\theta = 10°$; (b) $\theta = 15°$; (c) $\theta = 30°$; (d) $\theta = 45°$; (e) $\theta = 90°$.

were formulated by means of the dissipation function based on the invariant using a simple quadratic form of stress components.

To deal with the problem raised above in the present study, the effective stress and effective plastic strain proposed by Sun and Chen [12] is modified so as to consider

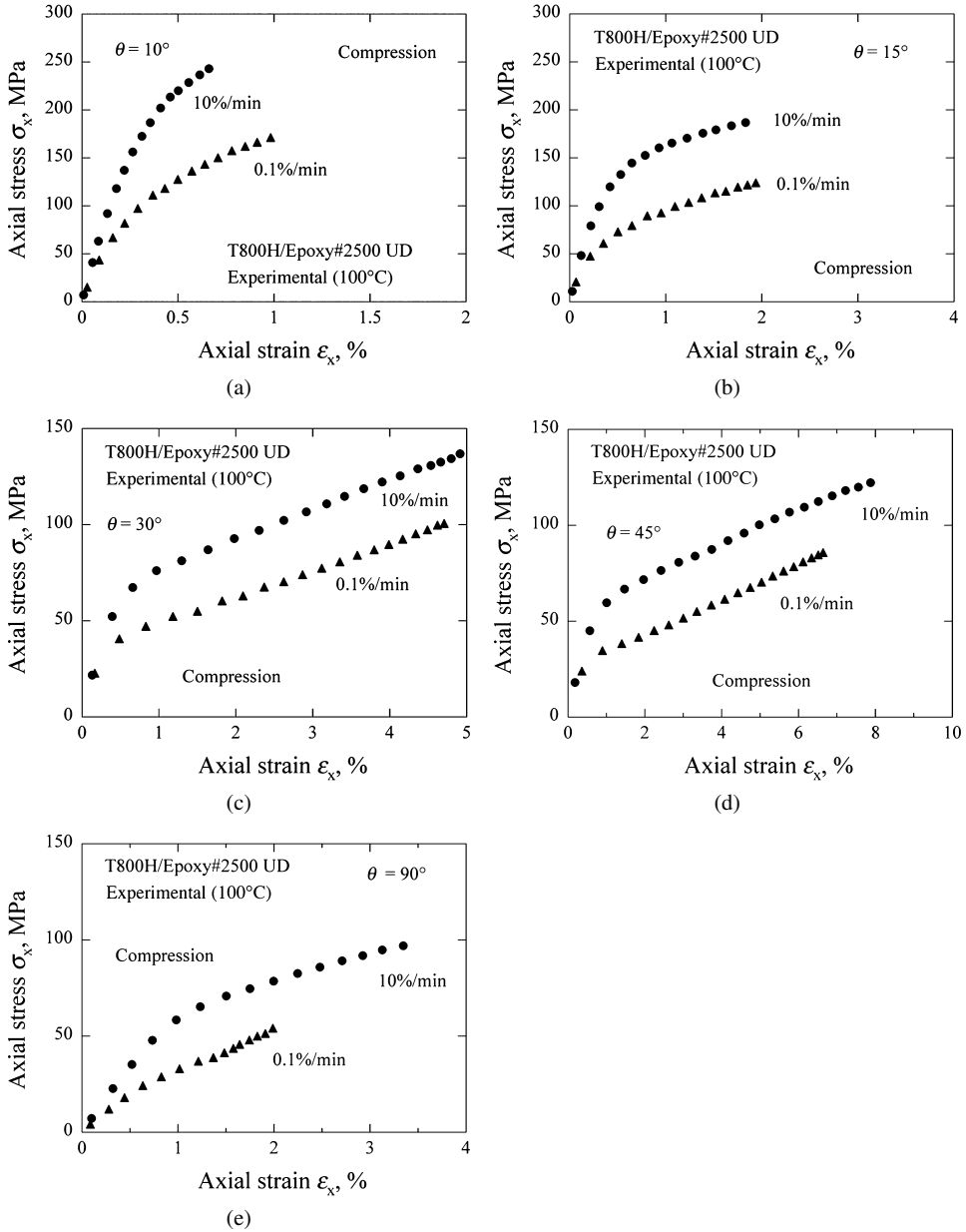

Figure 6. Comparison of off-axis compressive stress–strain curves at different strain rates (10%/min, 0.1%/min): (a) $\theta = 10°$; (b) $\theta = 15°$; (c) $\theta = 30°$; (d) $\theta = 45°$; (e) $\theta = 90°$.

the sign of transverse normal stress. By means of the extended effective stress and the effective viscoplastic strain rate, the isotropic-hardening viscoplasticity model [22–24] for unidirectional composites is generalized so that it is furnished with an enhanced capability to describe the different nonlinear deformation behaviors of

Table 2.
Apparent Young's modulus in tension and compression (0.1%/min)

Angle (°)	E_χ (GPa)	
	Tension	Compression
0	163.3	119.3
10	48.4	58.1
15	24.7	28.8
30	9.0	16.7
45	5.2	9.8
90	4.8	5.8

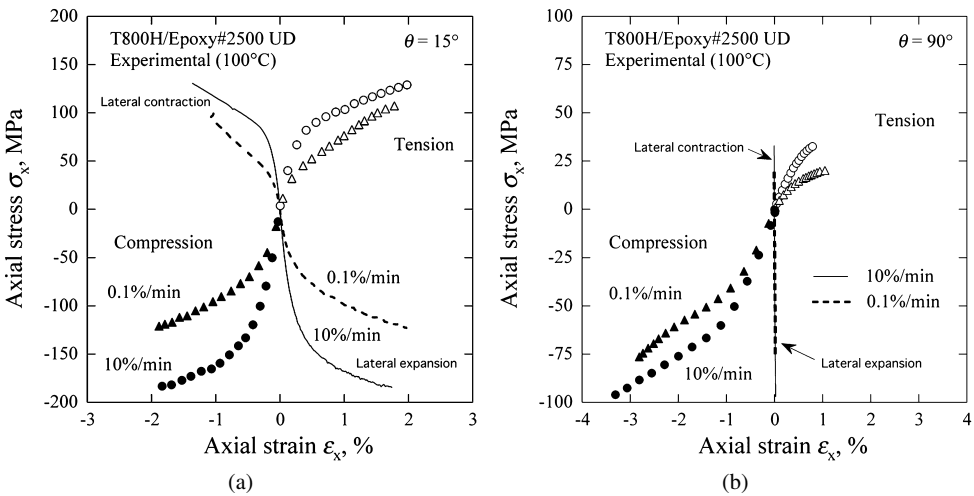

Figure 7. Overall axial and lateral behaviors under tensile and compressive loading at different strain rates (10%/min, 0.1%/min): (a) $\theta = 15°$; (b) $\theta = 90°$.

unidirectional composites under off-axis tension and compression. No yielding is assumed in the fiber direction as in the Sun–Chen plasticity model. The extended viscoplasticity model is tested for predictive accuracy by comparing predicted and experimental results.

A plane stress formulation is attempted in this study, and the associated stress and plastic strain rate vectors are defined as:

$$\boldsymbol{\sigma} = \{\sigma_{11}, \sigma_{22}, \tau_{12}\}^T, \tag{1}$$

$$\dot{\boldsymbol{\varepsilon}}^{\mathrm{p}} = \left\{\dot{\varepsilon}^{\mathrm{p}}_{11}, \dot{\varepsilon}^{\mathrm{p}}_{22}, \dot{\gamma}^{\mathrm{p}}_{12}\right\}^T, \tag{2}$$

where vector components are taken with respect to the principal material coordinate system. The inner product of two vectors $\mathbf{x}$, $\mathbf{y}$ is denoted as $\mathbf{x} \cdot \mathbf{y}$.

4.1. Effective Stress and Effective Plastic Strain

The effective stress proposed by Sun and Chen [12] is expressed as:

$$\bar{\sigma}_{\mathrm{SC}} = \sqrt{\frac{3}{2}\left[\sigma_{22}^2 + 2a_{66}\sigma_{12}^2\right]}, \tag{3}$$

where a_{66} is a material constant. To consider the effect of the sign of transverse normal stress in the present study, the effective stress is modified as:

$$\bar{\sigma} = \sqrt{\frac{3}{2}\boldsymbol{\sigma} \cdot \mathbf{B}\boldsymbol{\sigma}}, \tag{4}$$

where

$$\mathbf{B} = \begin{bmatrix} 0 & 0 & 0 \\ 0 & b_{22} & 0 \\ 0 & 0 & b_{66} \end{bmatrix} = \begin{bmatrix} 0 & 0 & 0 \\ 0 & \gamma & 0 \\ 0 & 0 & 2a_{66}\gamma \end{bmatrix}, \tag{5}$$

$$b_{22} = \gamma, \tag{6}$$

$$b_{66} = 2a_{66}\gamma, \tag{7}$$

$$\gamma = (1-c)H(\sigma_{22}) + c. \tag{8}$$

The sign of transverse normal stress is dealt with by means of the Heaviside function $H(x)$ which is defined as:

$$H(x) = \begin{cases} 1, & x \geqslant 0, \\ 0, & x < 0. \end{cases} \tag{9}$$

The modified effective stress takes different values according to the sign of the transverse stress component, and they are calculated as:

$$\bar{\sigma} = \begin{cases} \sqrt{\dfrac{3}{2}\left[\sigma_{22}^2 + 2a_{66}\sigma_{12}^2\right]}, & \sigma_{22} \geqslant 0, \\ \sqrt{\dfrac{3}{2}c\left[\sigma_{22}^2 + 2a_{66}\sigma_{12}^2\right]}, & \sigma_{22} < 0. \end{cases} \tag{10}$$

The additional parameter c represents the degree of different behaviors in tension and compression. In a particular case that $c = 1$, the modified effective stress is reduced to the original form given by Sun and Chen. Note that similar modification can be considered in a more general context for extension of a three-dimensional constitutive model.

4.2. An Extended Viscoplasticity Model

An isotropic hardening model that can describe the different nonlinear rate-dependent behaviors of unidirectional composites under tensile and compressive loading conditions is formulated on the basis of the irreversible thermodynamics with internal variables [25–27]. A dissipation potential from which the evolution

equations of assumed variables are derived is defined as a function of the modified effective stress presented above. Unidirectional fiber-reinforced composites are treated as homogeneous, transversely isotropic media. In the present paper, we limit our discussion to a quasi-isothermal inelastic process in which temperature and temperature gradient terms are negligible. An infinitesimal deformation is assumed, and the total strain is then expressed by the sum of the elastic and inelastic components; $\boldsymbol{\varepsilon} = \boldsymbol{\varepsilon}^{\mathrm{e}} + \boldsymbol{\varepsilon}^{\mathrm{p}}$.

4.2.1. Internal Variable and Associated Thermodynamic Force

A nonlinear characteristic of the viscoplastic deformation of homogenized transversely isotropic media is described by means of a scalar internal variable ρ. Assuming uncoupling between elasticity and viscoplasticity, we can express the Helmholtz free energy ψ to define the thermodynamic force associated with the internal variable as:

$$\psi = \psi_{\mathrm{e}}(\boldsymbol{\varepsilon}^{\mathrm{e}}) + \psi_{\mathrm{p}}(\rho). \tag{11}$$

The free energy components in the right-hand side of equation (11) are specified as

$$\psi_{\mathrm{e}}(\boldsymbol{\varepsilon}^{\mathrm{e}}) = \frac{1}{2}\boldsymbol{\varepsilon}^{\mathrm{e}} \cdot \mathbf{Q}\boldsymbol{\varepsilon}^{\mathrm{e}}, \tag{12}$$

$$\psi_{\mathrm{p}}(\rho) = h(\rho), \tag{13}$$

where $\mathbf{Q}$ is the elastic tensor of the material. The positive scalar function $h(\rho)$ plays a role to define a hardening variable that describes the nonlinearity of stress–strain relationship, and a particular form is assumed later on.

From the Helmholtz free energy function, we can derive Hooke's law and a relationship between the internal variable ρ and the associated thermodynamic force r (i.e., a hardening variable) as:

$$\boldsymbol{\sigma} = \frac{\partial \psi}{\partial \boldsymbol{\varepsilon}^{\mathrm{e}}} = \mathbf{Q}(\boldsymbol{\varepsilon} - \boldsymbol{\varepsilon}^{\mathrm{p}}), \tag{14}$$

$$r = \frac{\partial \psi}{\partial \rho} = \frac{\partial h}{\partial \rho}. \tag{15}$$

Using the effective stress and the hardening variable r, we can define an effective overstress $\overline{H}$ as:

$$\overline{H} = \bar{\sigma} - r - r_0, \tag{16}$$

where r_0 characterizes an initial elastic response, and it may be treated as an initial value of r. The effective overstress $\overline{H}$ represents the magnitude of a net stress that determines the magnitude of viscoplastic strain rate.

4.2.2. Evolution Equation

The evolution equations of the viscoplastic strain and internal variable are prescribed so as to satisfy the condition of positive mechanical dissipation:

$$D = \boldsymbol{\sigma} \cdot \dot{\boldsymbol{\varepsilon}}^{\mathrm{p}} - r\dot{\rho} \geqslant 0. \tag{17}$$

To meet this inequality, a convex dissipation function is defined as:

$$\Omega = \frac{m}{m+1}\left\langle \frac{\overline{H}}{K} \right\rangle^{(m+1)/m}, \tag{18}$$

where K, m are material constants. The angular brackets in equation (18), often called the Macaulay brackets, represent the function defined as $\langle x \rangle = \max\{0, x\} = x$ $(x \geqslant 0)$; 0 $(x < 0)$. Using the normality condition for the dissipation function, we can derive the viscoplastic strain rate and internal variable rate as follows:

$$\dot{\boldsymbol{\varepsilon}}^{\mathrm{p}} = \frac{\partial \Omega}{\partial \boldsymbol{\sigma}} = \dot{\lambda}\frac{3}{2}\frac{\mathbf{B}\boldsymbol{\sigma}}{\bar{\sigma}}, \tag{19}$$

$$\dot{\rho} = -\frac{\partial \Omega}{\partial r} = \dot{\lambda}, \tag{20}$$

where:

$$\dot{\lambda} = \left\langle \frac{\overline{H}}{K} \right\rangle^{1/m}. \tag{21}$$

The rate of viscoplastic work is given as:

$$\dot{W}^{\mathrm{p}} = \bar{\sigma}\,\bar{\dot{\varepsilon}}^{\mathrm{p}} = \boldsymbol{\sigma} \cdot \dot{\boldsymbol{\varepsilon}}^{\mathrm{p}}, \tag{22}$$

proving that the effective viscoplastic strain rate $\bar{\dot{\varepsilon}}^{\mathrm{p}}$ should agree with the positive multiplier $\dot{\lambda}$:

$$\bar{\dot{\varepsilon}}^{\mathrm{p}} = \dot{\lambda}. \tag{23}$$

Taking into account that the effective stress and effective viscoplastic strain rate are energy conjugate with each other, we can derive the expression of the effective viscoplastic strain rate as:

$$\bar{\dot{\varepsilon}}^{\mathrm{p}} = \sqrt{\frac{2}{3}\left[\frac{1}{b_{22}}(\dot{\varepsilon}_{22}^{\mathrm{p}})^2 + \frac{1}{b_{66}}(\dot{\gamma}_{12}^{\mathrm{p}})^2\right]}. \tag{24}$$

Note that for tensile loading in a given off-axis direction the extended effective stress and effective viscoplastic strain rate coincide with the definitions given by Sun and Chen [12]. It is also important that the assumption of no plastic strain appearing in the fiber direction has been preserved in the present formulation of viscoplasticity.

4.2.3. Hardening Variable

To establish a practical form of the evolution equation of the hardening variable, we need to give the state relation between ρ and r which is specified by the scalar function $h(\rho)$ in (13). Following Chaboche [28], we assume the scalar function as:

$$h(\rho) = Q\rho - \frac{Q}{b}[1 - \mathrm{e}^{-b\rho}], \tag{25}$$

where Q characterizes the saturation value of r, and b determines how quickly the isotropic hardening saturates with the accumulation of viscoplastic strain. From the definition, we can obtain the state relation of the exponential form:

$$r = Q(1 - \mathrm{e}^{-b\rho}), \tag{26}$$

where:

$$\rho = \bar{\varepsilon}^{\mathrm{p}} = \int \dot{\bar{\varepsilon}}^{\mathrm{p}}\,\mathrm{d}t. \tag{27}$$

Differentiation of (26) with respect to time leads to the following evolution equation [28]:

$$\dot{r} = b(Q - r)\dot{\bar{\varepsilon}}^{\mathrm{p}}. \tag{28}$$

The accuracy of prediction of the nonlinear hardening behavior can be enhanced by superposing the same type of variables characterized by the evolution equations with different nonlinearities [28]:

$$\dot{r} = \sum_a \dot{r}^{(a)} = \sum_a b^{(a)}(Q^{(a)} - r^{(a)})\dot{\bar{\varepsilon}}^{\mathrm{p}}. \tag{29}$$

Normally, two or three components are sufficient to accurately reproduce the nonlinear stress–strain behavior under simple proportional loading conditions.

4.2.4. Formulae for Off-Axis Loading

On simple loading along the x-axis, the effective stress and effective viscoplastic strain rate can be expressed as:

$$\bar{\sigma} = \sigma_x h(\theta), \tag{30}$$

$$\dot{\bar{\varepsilon}}^{\mathrm{p}} = \frac{1}{h(\theta)}\dot{\varepsilon}_x^{\mathrm{p}}, \tag{31}$$

where σ_x, $\dot{\varepsilon}_x^{\mathrm{p}}$ stand for the axial stress and axial viscoplastic strain rate, respectively, and

$$h(\theta) = \sqrt{\frac{3}{2}\left[b_{22}\sin^4\theta + b_{66}\cos^2\theta\sin^2\theta\right]}. \tag{32}$$

Using these formulae, we can express the total strain rate in the loading direction as:

$$\dot{\varepsilon}_x = \frac{1}{E_x}\dot{\sigma}_x + h(\theta)\left\langle\frac{h(\theta)\sigma_x - r - \sigma_0}{K}\right\rangle^{1/m}, \tag{33}$$

where E_x is the Young's modulus in the loading direction. Note that the viscoplasticity model presented in this study differs from the Gates–Sun model in the definition of the effective stress and strain and it leads to a different form of orientation function $h(\theta)$, although they share a common form of the uniaxial formula given by (33).

Table 3.
Engineering elastic constants for the unidirectional T800H/2500 carbon/epoxy composite at 100°C

Test conditions		Engineering elastic constants			
		E_1 (GPa)	E_2 (GPa)	G_{12} (GPa)	υ_{12}
10%/min	Tension	163.5	6.5	3.0	0.379
	Compression	146.6	6.9	3.8	0.322
0.1%/min	Tension	163.3	4.8	2.0	0.382
	Compression	119.3	5.8	3.5	0.303

4.3. Verification

4.3.1. Material Identification

In the case of tensile loading, the parameter γ takes the value of unity; $\gamma = 1$. The modified effective stress is then reduced to the original form given by Sun and Chen, and the viscoplasticity model that considers the tension–compression asymmetry is reduced to the tension–compression symmetry model tested in the previous studies [22–24]. As a result, all the material constants involved except for the additional constant c can be determined on the basis of the off-axis tensile behavior. The detailed procedure for their identification can be found in the previous reports [22–24]. The value of c is roughly evaluated first by comparing the yield stress levels in tension and compression, and then it is modified so as to improve the accuracy of prediction of the compressive stress–strain curve for $\theta = 90°$. The values of the material constants involved by the tension–compression asymmetry model developed in this study were finally identified as $K = 81$ MPa min, $m = 0.19$, $r_0 = 0$ MPa, $Q_1 = 45$ MPa, $Q_2 = 40.5$ MPa, $Q_3 = 18$ MPa, $b_1 = 40$, $b_2 = 10$, $b_3 = 5$, $a_{66} = 2.2$ and $c = 0.78$. The engineering elastic constants obtained from the tension and compression tests at 10%/min and 0.1%/min are listed in Table 3.

4.3.2. Comparison with Experimental Results

Comparisons of the predicted and observed off-axis tensile and compressive stress–strain curves at the two strain rates of 10%/min and 0.1%/min are shown in Fig. 8(a)–8(e) for all fiber orientations, respectively. We can see that the characteristic features of the off-axis nonlinear behavior, i.e., the different behaviors in tension and compression, the fiber-orientation dependence of stress–strain curves and their strain rate dependence, have successfully been predicted using the proposed viscoplasticity model. It is emphasized that all these predictions have been obtained by means of a single viscoplasticity model.

Validity of the proposed viscoplasticity model for applicability to different kinds of polymer matrix composites should be tested further. For a class of carbon/epoxy system similar to the material used in this study, however, it is expected that the proposed viscoplasticity model may be used in a preliminary design-by-analysis of composite elements subjected to off-axis tension and compression. The mechanism

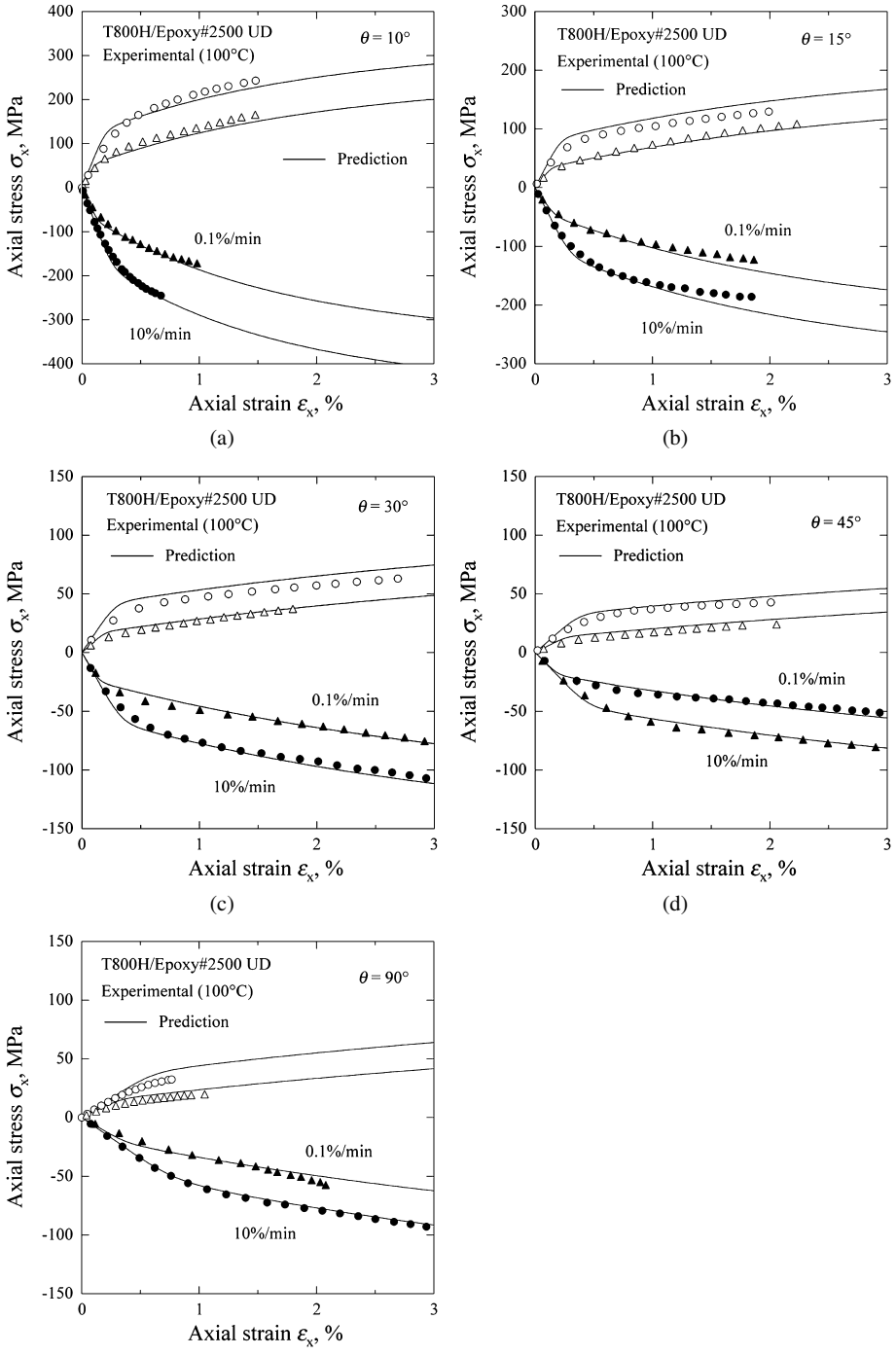

Figure 8. Predicted off-axis tensile and compressive stress–strain curves at different strain rates (10%/min, 0.1%/min): (a) $\theta = 10°$; (b) $\theta = 15°$; (c) $\theta = 30°$; (d) $\theta = 45°$; (e) $\theta = 90°$.

devised to modify the effective stress in this study may also be used for developing a multiaxial constitutive model that takes into account the tension–compression asymmetry of the viscoplastic behavior of unidirectional composites under more general loading conditions.

5. Conclusion

The similarity and difference in flow stress level, nonlinearity of stress–strain response and strain-rate dependence between the off-axis tensile and compressive deformation behaviors of a unidirectional T800H/2500 carbon/epoxy composite at 100°C were elucidated. Formulation of a viscoplastic constitutive model for unidirectional composites that can describe not only the fiber-orientation dependence of off-axis nonlinear rate-dependent behavior but also the off-axis flow stress differential in tension and compression was attempted. The validity of the proposed viscoplasticity model was evaluated by comparing predicted and observed off-axis tensile and compressive behaviors at different strain rates. The results obtained can be summarized as follows:

(1) The off-axis tensile and compressive deformation behaviors showed similar nonlinearity and fiber-orientation dependence. A feature that distinguished the off-axis compressive behavior from the off-axis tensile behavior was that the compressive stress–strain relationship for $\theta = 90°$ crossed with that for $\theta = 45°$. In the case of transverse compression, the ultimate failure is retarded due to the suppression of separation failure by the transverse compressive stress, which allows the axial stress in the 90° specimen to ultimately reach a higher level than in the 45° specimen. The effect of the separation failure suppression due to the action of transverse compressive stress was also reflected by the increase in failure strain especially for the fiber orientations $\theta = 30°, 45°$.

(2) The off-axis flow stress at a lower strain rate becomes smaller than the value at a higher strain rate both in tension and compression, regardless of the fiber orientation. Similar rate dependence was seen in the off-axis nonlinear behaviors under tensile and compressive loading conditions.

(3) The off-axis compressive flow stress was larger than the off-axis tensile flow stress, regardless of the off-axis fiber orientation. Such a tension–compression asymmetry was observed at different strain rates. There was a tendency for the ratio of the compressive flow stress to the tensile one to increase with increasing off-axis angle.

(4) The off-axis behaviors at the different strain rates of 10%/min and 0.1%/min were overall similar in nonlinearity, fiber-orientation dependence and tension–compression asymmetry.

(5) A viscoplasticity model to describe the tension–compression asymmetry in the off-axis nonlinear rate-dependent behavior of unidirectional composites was

developed. The formulation was based on a modified form of the effective stress introduced by Sun and Chen, and a simple mechanism to allow a different magnitude of the effective stress in tension and compression was considered.

(6) The fiber-orientation dependence, the tension–compression asymmetry and the strain-rate dependence in the off-axis nonlinear deformation of the unidirectional carbon/epoxy laminate at 100°C can be predicted using the proposed viscoplasticity model.

Acknowledgement

The authors gratefully acknowledge financial support provided in part by JAXA and the University of Tsukuba under a research corporation program CCD19158.

References

1. H. F. Brinson, Matrix dominated time dependent failure predictions in polymer matrix composites, *Compos. Struct.* **47**, 445–456 (1999).
2. L. H. V. Vlack, *Materials Science for Engineers*. Addison-Wesley, Massachusetts, MA, USA (1970).
3. C. R. Barrett, W. D. Nix and A. S. Tetelman, *The Principles of Engineering Materials*. Prentice-Hall, Englewood Cliffs, UK (1973).
4. T. H. Courtney, *Mechanical Behavior of Materials*. McGraw-Hill, Singapore (1990).
5. S. Matsuoka, *Relaxation Phenomena in Polymers*. Oxford University Press, New York, USA (1992).
6. L. E. Nielsen, *Mechanical Properties of Polymers and Composites*. Marcel Dekker, New York, USA (1975).
7. R. M. Caddell, R. S. Raghava and A. G. Atkins, A yield criterion for anisotropic and pressure dependent solids such as oriented polymers, *J. Mater. Sci.* **8**, 1641–1646 (1973).
8. T. S. Gates and C. T. Sun, Elastic/viscoplastic constitutive model for fiber reinforced thermoplastic composites, *AIAA J.* **29**, 457–463 (1991).
9. M. Kawai, Y. Masuko, Y. Kawase and R. Negishi, Micromechanical analysis of the off-axis rate-dependent inelastic behavior of unidirectional AS4/PEEK at high temperature, *Intl J. Mech. Sci.* **43**, 2069–2090 (2001).
10. C. T. Sun and K. J. Yoon, Characterization of elastic–plastic behavior of AS4/PEEK thermoplastic composite for temperature variation, *J. Compos. Mater.* **25**, 1297–1313 (1991).
11. J. Tsai and C. T. Sun, Constitutive model for high strain rate response of polymeric composites, *Compos. Sci. Technol.* **62**, 1289–1297 (2002).
12. C. T. Sun and J. L. Chen, A simple flow rule for characterizing nonlinear behavior of fiber composites, *J. Compos. Mater.* **23**, 1009–1020 (1989).
13. K. J. Yoon and C. T. Sun, Characterization of elastic–plastic behavior of an AS4/PEEK thermoplastic composite, *J. Compos. Mater.* **25**, 1277–1296 (1991).
14. S. R. Bodner and Y. Partom, Constitutive equations for elastic–viscoplastic strain-hardening materials, *ASME J. Appl. Mech.* **42**, 385–389 (1975).
15. C. Wang and C. T. Sun, Experimental characterization of constitutive models for PEEK thermoplastic composite at heating stage during forming, *J. Compos. Mater.* **31**, 1480–1506 (1997).

16. JIS K7073, *Testing Method for Tensile Properties of Carbon Fiber-Reinforced Plastics*, Japanese Industrial Standard, Japanese Standards Association (1988).
17. JIS K7076, *A Compression Examination Method in Respect of CFRP*, Japanese Industrial Standard, Japanese Industrial Association (1991).
18. J. G. Haberle and F. L. Matthews, An improved technique for compression testing of unidirectional fibre-reinforced plastics: development and results, *Composites Part A* **25**, 358–371 (1994).
19. H. M. Hsiao and I. M. Daniel, Effect of fiber waviness on stiffness and strength reduction of unidirectional composites under compressive loading, *Compos. Sci. Technol.* **56**, 581–593 (1996).
20. M. Kawai and S. Saito, Off-axis strength differential effect in unidirectional carbon/epoxy laminates at high temperature and failure envelope prediction (in preparation) (2008).
21. S. K. Ha and G. S. Springer, Time dependent behavior of laminated composite at elevated temperature, *J. Compos. Mater.* **23**, 1159–1197 (1989).
22. M. Kawai and Y. Masuko, Creep behavior of unidirectional and angle-ply T800H/3631 laminates at high temperature and simulation using a phenomenological viscoplasticity model, *Compos. Sci. Technol.* **64**, 2373–2384 (2004).
23. Y. Masuko and M. Kawai, Application of a phenomenological viscoplasticity model to the stress relaxation behavior of unidirectional and angle-ply CFRP laminates at high temperature, *Composites Part A* **35**, 817–826 (2004).
24. F. Takeuchi, M. Kawai, J. Q. Zhang and T. Matsuda, Rate-dependence of off-axis tensile behavior of cross-ply CFRP laminates at elevated temperature and its simulation, *Adv. Compos. Mater.* **17**, 57–73 (2008).
25. J. Lemaitre and J. L. Chaboche, *Mechanics of Solid Materials*. Cambridge University Press, Cambridge, UK (1985).
26. M. Kawai, Constitutive model for coupled inelasticity and damage, *JSME Intl J. Series A* **39**, 508–516 (1996).
27. M. Kawai and Y. Masuko, Macromechanical modeling and analysis of the viscoplastic behavior of unidirectional fiber-reinforced composites, *J. Compos. Mater.* **37**, 1885–1902 (2003).
28. J. L. Chaboche, Viscoplastic constitutive equations for the description of cyclic and anisotropic behavior of metals, *Bulletin de L'Academie Polonaise des Science, Série de Science Techniques* **25**, 33–42 (1977).